Available online at www.sciencedirect.com
ScienceDirect
Polymer 49 (2008) 303–316
polymer
www.elsevier.com/locate/polymer

Orientation of polyoxymethylene by rolling with side constraints

J. Mohanraj [a,1], J. Morawiec [b], A. Pawlak [b], D.C. Barton [a], A. Galeski [b,*], I.M. Ward [c]

[a] School of Mechanical Engineering, University of Leeds, Leeds LS2 9JT, UK
[b] Centre of Molecular and Macromolecular Studies, Polish Academy of Sciences, Sienkiewicza 112, 90-363 Lodz, Poland
[c] School of Physics and Astronomy, University of Leeds, Leeds LS2 9JT, UK

Received 4 July 2007; received in revised form 30 October 2007; accepted 6 November 2007
Available online 7 November 2007

Abstract

In this paper, we describe the application of the constrained rolling process to produce highly oriented polyacetal bars with enhanced mechanical properties. In this process, the heated polymer billet is deformed in a channel formed in the circumference of the bottom roll that provides lateral constraint to the material as it deforms. It is a process that has attracted interest due to its capability to produce thick cross-sectional oriented products continuously and at moderate production speeds. Here the focus is on two commercial grades of polyoxymethylene (a) Delrin® 100 and (b) Tarnoform® 300. Tarnoform®, unlike Delrin®, is a copolymer. The compression behaviour of these grades has been investigated in a plane strain channel die to determine the optimum constrained rolling conditions. Samples were then rolled to different reduction ratios close to but below the crystalline melting temperature of the two grades.

The modulus and strength increased almost linearly with reduction ratio. Rolled Delrin® exhibited higher modulus and strength than Tarnoform®. Under impact loading, with the initial notch perpendicular to the rolling direction, the fracture process was incomplete for both resins with the specimens exhibiting a hinge type break. Structural investigations of the rolled samples were carried out by wide and small angle X-ray diffraction. The structures produced were very similar to those produced in plane strain compression test. The pole figures from the (100) reflection suggest that the *c* axes of the POM crystals are oriented along the rolling direction while *ab* planes showed clustering of orientation of (100) normals in six directions. SAXS patterns from the rolled samples with the X-ray beam parallel to the force direction showed two-point patterns that suggest the transformation of the spherulitic morphology to a fibrillar structure in this direction. However, perpendicular to the rolling direction, four-point patterns were obtained that suggest cooperative kinking of the lamellae during deformation to produce a chevron-like structure. The enhancement in properties as a result of molecular orientation suggests that these materials can have major commercial applications.

Keywords: Polyoxymethylene; Rolling; Plane strain compression

1. Introduction

Molecular orientation in polymers greatly improves their mechanical and physical properties compared to the isotropic material [1–5]. Oriented polymers have found extensive applications in the production of fibres, films, pipes, sheets, etc. and recently more complex profiles have been manufactured.

Molecular orientation in polymers can be achieved by processing either in the melt or in the solid state. The enhancement of properties in the melt state is low due to the high temperature of the melt and the shaping device that increases the mobility of the molecular chains. However, in the solid-state processes, the molecular chains are essentially ''frozen-in'' leading to significant enhancements in the properties. In these processes, the polymers are processed below the crystalline melting temperature in the case of semi-crystalline polymer or near the glass transition temperature for amorphous polymer. Examples of solid-state orientation processes include tensile free drawing, die-drawing, hydrostatic extrusion, rolling, roll-drawing, constrained rolling process and equal

* Corresponding author. Tel.: +48 42 6803250; fax: +48 42 6803261.
E-mail address: andgal@bilbo.cbmm.lodz.pl (A. Galeski).
[1] Present address: Bridon, Carr Hill, Doncaster DN4 8DG, UK.

0032-3861/$ - see front matter © 2007 Elsevier Ltd. All rights reserved.
doi:10.1016/j.polymer.2007.11.008

channel extrusion process. A review of the above processes can be found in the literature [4–7].

The solid-state orientation processes can be broadly classified into two based on the stress state of the material in the shaping device. In the case of a tensile deformation process such as tensile free drawing and die-drawing, high production rates have been achieved [8]. However, the tensile nature of the processes causes structural damage in the material that lowers the fracture strength [9,10] of the oriented polymer. Fracture occurs when the flow stress, which increases with speed due to strain rate sensitivity, exceeds the fracture strength of the material. In the case of a compressive deformation process, the flow stress increases with strain and also due to the increased effect of the hydrostatic component of stress [11], which is counterproductive in terms of production speed. However, structural defects are minimised due to the compressive nature of the stresses in the material induced by the shaping device and this enhances the strength of the oriented polymer.

In this work the focus is on polyoxymethylene (POM), a polymer which has previously been oriented in the solid state by different routes and significant enhancements in modulus and strength have been obtained [9,12–14]. For example, a modulus of 58 GPa and strength as high as 2 GPa have been achieved by solid-state deformation of the polymer under hydrostatic pressure [9]. Oriented POM also offers superior resistance to creep [15], low coefficient of thermal expansion [16], heat shrinkage [17] and offers good chemical resistance [18]. Previous research has shown that this material in the oriented form is susceptible to structural damage such as voids [10,19,20], the extent of which has been shown to be influenced by the total plastic strain and the strain rate [21].

In this paper, we report the structure and properties of two commercial grades of polyoxymethylene oriented by the constrained rolling process. Polyoxymethylene has previously only been oriented by the conventional rolling process. Rolling thick cross-section polymer close to the melt temperature without side constraints can cause unnecessary transverse deformation and can lead to edge defects in the rolled material like fissures, edge cracking, warping, etc. [22]. This limits the conventional rolling process essentially to thin and wide strips of the material. In the constrained rolling process, the heated polymer billet is deformed in the channel formed between the circumference of the bottom-grooved roll and the top roll as schematically shown in Fig. 1. The channel in the bottom-grooved roll provides lateral constraint to the material as it deforms, which prevents transverse deformation and hence the formation of edge defects in the material. The top roll is of the same width as the channel and acts in effect as a plunger. The advantage of this process is its ability to orient relatively thick cross-section material continuously. This process has previously been used to orient a number of polymers [23–26]. Significant improvements in the modulus, strength and impact properties over the isotropic material have been reported for both polyethylene [24,25] and polypropylene [26]. However, no such studies have been reported for polyoxymethylene.

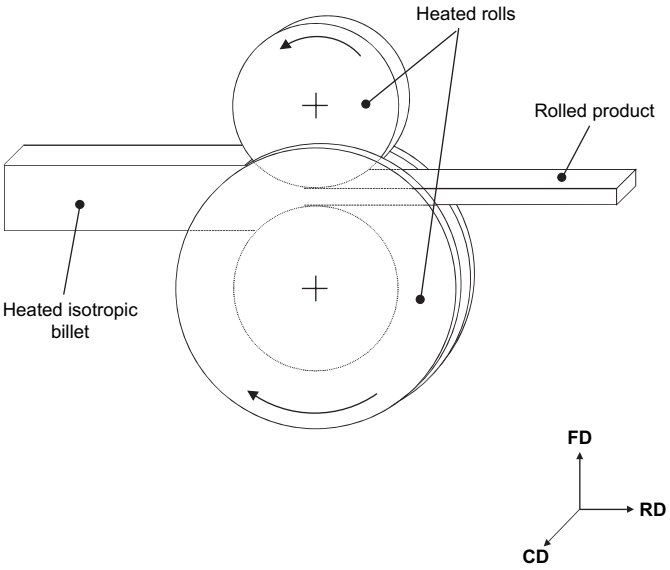

Fig. 1. Schematic of the constrained rolling process.

2. Experimental procedures

2.1. Materials

Two materials were used in this study. They are (a) Delrin® 100 by DuPont Engineering Polymers and (b) Tarnoform® 300 by Zaklady Azotowe Tarnow (Poland). Tarnoform®, unlike Delrin®, which is a homopolymer, is a copolymer produced by polymerisation of trioxane and copolymerized with 2–3% of dioxolane, which acts as a stabiliser in the resin. The density, melt flow index of the materials used in this study are given in Table 1. The materials were supplied as extruded sheets of thickness 16 mm and were cut into billets 1 m long and with varied width.

2.2. Thermal characterization

The melting behaviour of the extruded Delrin® and Tarnoform samples was studied out using a TA 2920 (Thermal Analysis, New Castle, DE) analyser. Indium was used to calibrate the temperature and enthalpy. The crystalline melting temperature was determined at a heating rate of 10 °C/min under nitrogen atmosphere using a sample weight of 5–8 mg. The melting temperature reported here is an average from 5 scans.

2.3. Plane strain compression tests

It has been shown in the case of polypropylene and HDPE that the deformation behaviour of the material in the constrained rolling process matches the Plane Strain Compression (PSC)

Table 1
Details of the materials used in this study

Material	Density, g/cm^3	Melt flow index (190 °C; 2.16 kg)
Delrin® 100	1.427	3.9
Tarnoform® 300	1.41	5.68

process in a channel die [23]. Hence PSC tests were carried out in a channel die on Delrin® and Tarnoform® to establish the optimum conditions for the constrained rolling process. Details of the channel die tests are reported elsewhere [27]. For the PSC tests, samples of dimensions $50 \times 75 \times 4$ mm were cut from plates and compressed at different temperatures below the crystalline melting temperature of the polymer. The samples were tested in the channel die at different temperatures at a strain rate of 0.001 s^{-1}. Prior to the test, the die wall was lubricated with molybdenum sulphide to minimise the friction between the sample and the die faces during the test.

2.4. Constrained rolling

A photograph of the constrained rolling machine at the Polish Academy of Sciences, Lodz (Poland) is shown in Fig. 2. The set up consists of a series of pairs of rolls, as shown in the photograph, driven independently by electric motors through a gearbox unit. Since the rolls are independently driven, it is possible with this set up to simultaneously roll and axially deform the sample between the roll pairs, resembling the roll-drawing process [4,28,29]. For this work the speed of the second roll pair was adjusted to match the axial linear speed of the sample exiting the first roll pair in order to ensure that no tensile free drawing occurred between the pairs of rolls.

The outer diameter of the bottom rolls was 480 mm and the channel cut in the circumference was 100 mm deep and 12 mm wide. The diameter of the top rolls was 280 mm and the width was 12 mm, matching the channel in the bottom roll. The top rolls were mounted on a movable frame connected to a screw, which sets the amount of deformation during each rolling pass. The rolls and the spindles were made of hardened steel and were designed to withstand high stresses during the rolling process. The temperature of the bottom rolls was maintained by heating elements mounted in the rollers and controlled by independent temperature controllers. The top rolls were heated to the desired temperature by blowing hot air through a hot air gun.

The geometry of the deformation was characterized in terms of the nominal reduction ratio, R_N, defined as the ratio of the thickness of the start-up billet to the minimum gap between the top and the bottom rolls. The actual degree of deformation experienced by the material was expressed by the actual reduction ratio, R_A, which was defined as the ratio of the thickness of the initial billet to the thickness of the product. The deformation in the channel formed by the rolls is close to plane strain conditions due to the lateral constraints imposed on the material during the rolling process. Assuming that the deformation occurs at constant volume, the actual reduction ratio is related to the draw ratio of the material along the rolling direction. Thus, the deformation experienced by the polymer in the channel of the constrained rolling process is kinematically similar to the constant width slot tensile die-drawing of polymers.

Samples for the rolling trials were machined to a thickness of 12 mm to ensure slug fit in the channel formed on the lower roll. The thickness of the billets was varied to achieve different R_Ns. In a typical rolling trial, the rolls were first heated to the desired rolling temperature. A conical tag was machined at one end of the start-up billets to facilitate easy entry into the gap between the rolls. Deformation of the billet to a particular reduction ratio was carried out in many sequential steps of lower deformation. For example, about 10 passes were required to produce an R_A of around 6. The linear speeds of the two pairs of rolls were kept constant at 78 mm/min and 100 mm/min, respectively.

2.5. Structural characterization

For structural studies on the rolled POM, 2 mm thick rectangular strips were machined from the core of the rolled product perpendicular to the Constraint Direction (CD), Force Direction (FD) and Rolling Direction (RD). A 2 mm thick strip was machined from the initial extruded sheet in the direction of the extrusion for studies on isotropic POM.

2.5.1. WAXS

The wide-angle X-ray scattering (WAXS) studies on the isotropic and rolled POM samples were performed using a computer-controlled wide-angle diffractometer system

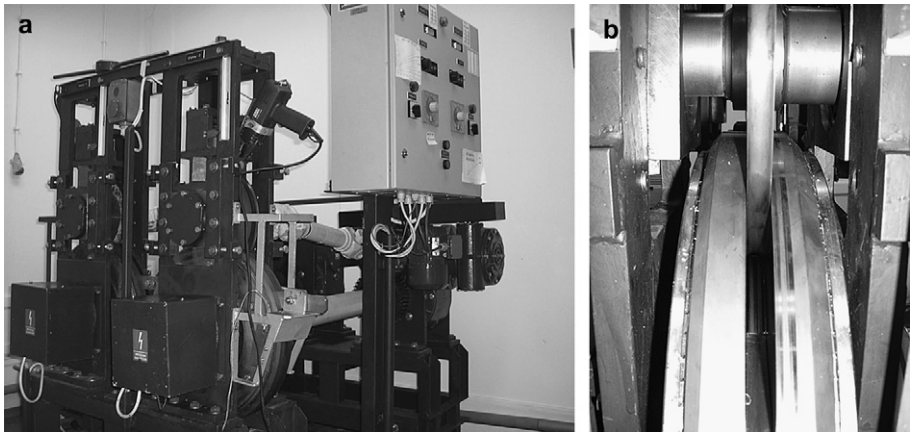

Fig. 2. Photograph of the constrained rolling machine at the Polish Academy of Sciences, Lodz (Poland). (a) Overview and (b) details of constrained rolls.

equipped with a pole figure attachment coupled to a sealed-tube source of filtered Cu Kα radiation of wavelength $\lambda = 1.542$ Å operating at 50 kV and 30 mA (Phillips). The 2θ scans were determined in transmission geometry in the angular range of 15°–60° in steps of 0.05°. The texture of the isotropic and oriented samples was studied by means of X-ray pole figures.

The crystalline orientation of the rolled samples was studied using the pole figure technique for the (100), (105), (115) and (205) planes at the 2θ diffraction angles of 22.9°, 34.5°, 48.2° and 54.1°, respectively.

The scans were performed in reflection mode for the projections of the Euler angles of the reference direction with respect to the incident beam of α varying from 0° to 90° and β varying from 0° to 360°, both in steps of 5°. Reflection mode was used for α up to 60° and transmission mode was used for α from 50° to 90°. The two data sets were merged at a connection angle of 50°. The data were corrected for air scattering (with no sample) and sample absorption in the relevant modes. After the corrections, the intensities from both modes were normalised to the same level and then merged into a single data set at an angle of 50° using the POD program, which is a part of the popLA package (Los Alamos Laboratory).

2.5.2. SAXS

The small angle X-ray scattering (SAXS) studies were performed at the Synchrotron Radiation Source, Daresbury (United Kingdom). The SAXS patterns were obtained on a multi-wire 2D detector using Cu Kα radiation of wavelength $\lambda = 1.41$ Å. The patterns were collected for 2 min at 20 °C. The detector to sample distance was fixed at 3.5 m with the beam stop positioned close to the detector. At the end of each scan, a background pattern was collected without the sample for the same duration and subtracted from the sample pattern.

2.6. Tensile tests

Dumbbell samples of gauge length 45 mm, width 8 mm and thickness 4 mm were machined from the isotropic and rolled sheets. The sample ends were gripped using 'V' shaped serrated grips and tested at 20 °C at a crosshead speed of 1 mm/min in an Instron universal testing machine. The modulus was determined from the initial elastic region using a video extensometer attached to the testing machine. The strength was determined by dividing the peak load in the load–displacement plot by the initial cross-sectional area of the sample. The modulus and strength values quoted here are an average of at least 5 tests.

2.7. Impact tests

The sample dimensions for the impact tests were of length 60 mm, width 10 mm and thickness 5 mm. Isotropic samples for the impact tests were machined from the extruded sheet parallel to the extrusion direction. Impact samples were machined from the rolled samples with the initial notch parallel to the Force Direction (FD) and Constraint Direction (CD). The samples were notched on one side of the sample half way along the length. The crack tips were then sharpened by gently tapping a fresh razor blade at the root of the notch. The ratio of crack length to specimen width was kept between 0.45 and 0.55 following the recommendations suggested in the testing protocol by the European Group on Fracture (EGF) [30]. The impact tests were performed in the Rosand instrumented impact-testing machine at 20 °C at 1 m/s. The load–displacement plots were downloaded and analyzed on a computer interfaced with the impact machine.

3. Results and discussion

3.1. Melting behaviour

Isotropic Delrin® had a melt temperature (T_M) of 179 °C with the onset of melting at approximately 155 °C. Isotropic Tarnoform® exhibited a T_M of 166 °C with the onset of melting at approximately 145 °C, both significantly lower than Delrin®. The heat of fusion of POM crystal was assumed to be 317.93 J/g [31]. The degree of crystallinity at the core of the extruded Delrin® and Tarnoform® was 55% and 48%, respectively.

3.2. Plane strain compression behaviour

Fig. 3 shows the stress–strain curves for Delrin® and Tarnoform® for the PSC tests in a channel die at different temperatures. After yield, the crosshead speed was varied with the aid of a feedback system to maintain a constant compression rate throughout the test. The flow stress increases as the test temperature is decreased as expected for a thermoplastic polymer. For both materials, the temperature has a strong influence on the stress and the maximum attainable strain. In the case of Delrin®, a maximum strain of 300%, which corresponds to a reduction ratio of 4.0 was achieved at 160 °C. In the case of Tarnoform®, the maximum strain of 300% corresponding to a R_A of 4.0 was achieved at a stress of less than 100 MPa. It was shown by Morawiec et al. [23] for polypropylene tested slightly below its melting temperature that a small increase of temperature has stronger influence on the maximum attainable strain than a change of the strain rate by a few orders of magnitude. Although the results are not shown here, similar observations were made for Delrin® and Tarnoform®. No visible fracture occurred in the samples, which were more translucent than the start-up material.

3.3. Rolling behaviour

An important consideration is the choice of rolling temperature for the two resins. Solid-state rolling should be performed below the T_M with allowance given for the heat generated due to the friction between the polymer and the rolls and the plastic work. Higher rolling temperatures, close to the T_M, provide the advantage of being able to achieve higher

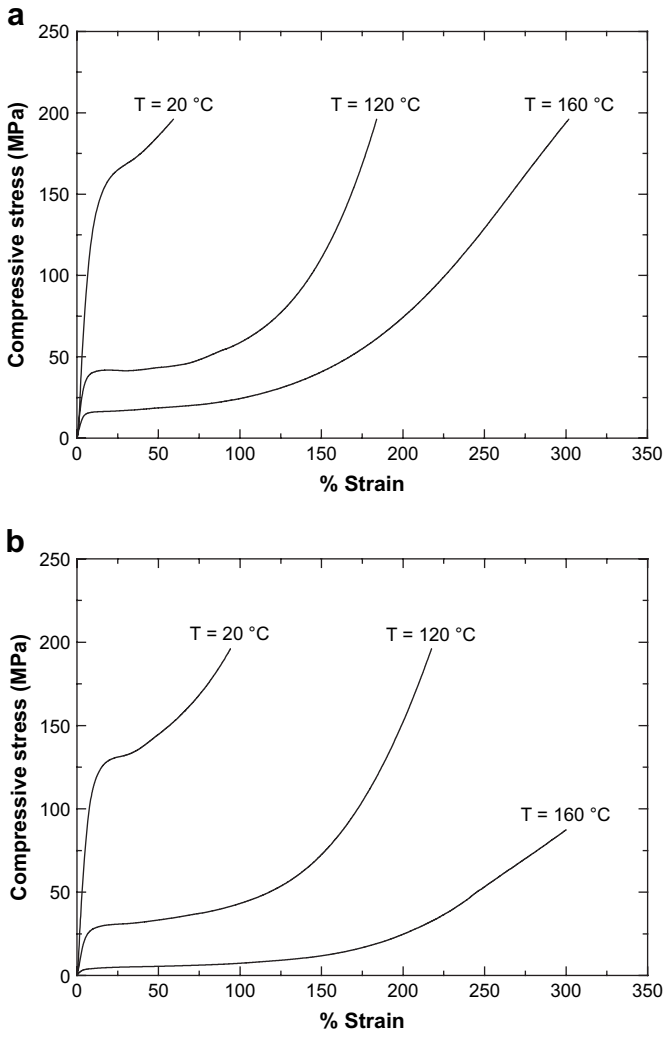

Fig. 3. Compressive stress–strain curves of (a) Delrin® and (b) Tarnoform® compressed in a channel die at a strain rate of 0.001 s^{-1} at different test temperatures.

reductions and at higher speeds. However, from the point of enhancement of properties, higher orientation temperatures permit some relaxation of the oriented structure, reducing its stiffness and strength. At lower draw temperatures, good property enhancement can be gained at lower reduction ratios since the amorphous and crystalline domains oriented in the roll direction are 'frozen' in this configuration as the product cools after exiting the rolls. Thus roll temperature has to be chosen such that the draw speed and property enhancement are both optimized. One objective of this work was to assess the behaviour of polyoxymethylene in the constrained rolling process at higher reduction ratios. Hence the rolling trials were performed close to T_M. From the PSC tests in the channel die, it was established that 160 °C was the optimum temperature to orient these resins in compression. In these tests, the friction between the polymer and the die was minimised by applying lubricant at the interface. However, rolling trials at 160 °C led to partial melting of the sample between the rolls during the deformation process, as a result of the heat generated due to friction. In the present study, the rolling trials on Delrin® were therefore performed at 145 °C while Tarnoform® was rolled at 135 °C due to its lower T_M.

Grid lines of known spacing were printed on the start-up billet on sides perpendicular to the Constraint Direction (CD) and parallel to the Force Direction (FD). Fig. 4(a) shows the photograph of a typical Delrin® sample rolled at 145 °C and extracted from the rolls after multiple passes to a R_A of around 3. At the entry to the rolls the grid lines curve in the rolling direction, which is as a result of the friction driving the material into the working zone between the rolls. Between the rolls, additional shearing was noticed in the direction of the rolling that could be due to the ''sticking friction'' phenomenon observed in the case of hot rolling of metals [32]. At temperatures close to the melting point of the material, the yield stress in shear is so low that moderate rolling pressure can cause significant shearing of the material.

The distance between the grid lines on the face perpendicular to the CD increased as a result of rolling. In addition in the central part of the specimen, shearing of the lines parallel to RD was also noticed. This observation suggests that the

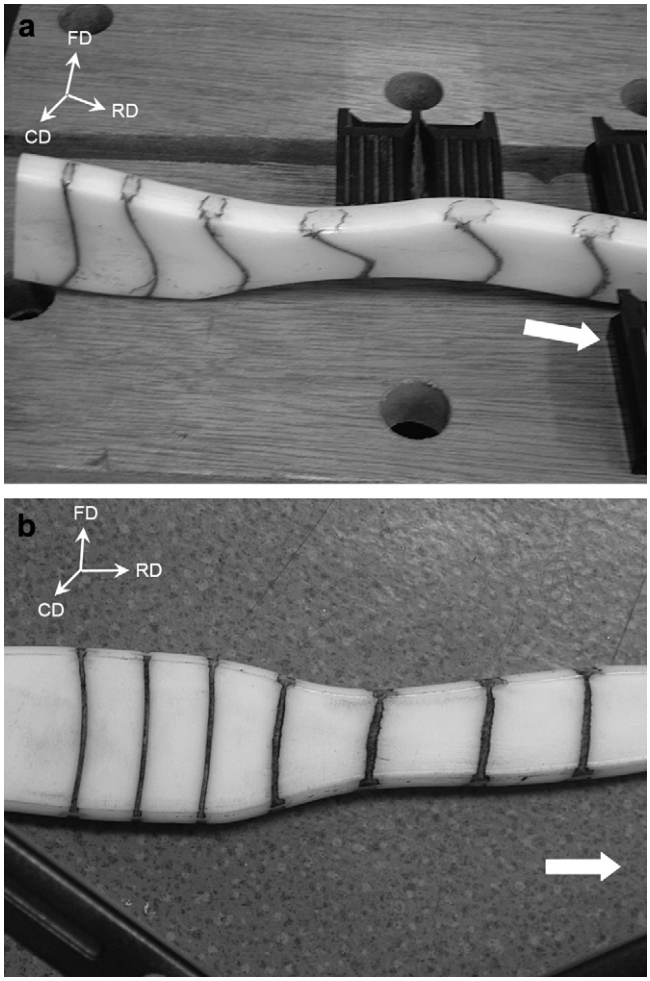

Fig. 4. Photograph of the samples of Delrin® rolled at (a) 145 °C and (b) 135 °C that was extracted from the rolls after compressing the sample to a R_A of around 3. Arrow in the figure indicates the rolling direction.

deformation of the billet between the roll gap is non-uniform through the thickness, with the maximum strain in the central part of the sample. The grid lines drawn on the face perpendicular to the FD in the CD–RD plane were extended along the RD as shown in Fig. 4(a) more than the lines in the FD–RD face near the rolled surface of the bar. This illustrates that the shear flow is more prevalent on the face that is in contact with the rolls. Although no fracture was noticed in the present case, it has previously been shown in the case of HDPE that the redundant deformation at high reduction ratios could lead to premature fracture of the sample by delamination in the plane perpendicular to the FD [24,26].

For the sake of comparison a sample of Delrin® was rolled at 135 °C, which is 10 °C lower than the earlier case as shown in Fig. 4(b). In this case, the grid lines ascribed normal to the CD remained plane even after excessive rolling, suggesting conditions approaching the ideal plane strain rolling case. The lower shearing of the material along the rolling direction could be due to relatively high shear yield stress of the material at this lower temperature.

Fig. 5(a) and (b) shows the % recovery in the samples after each rolling pass at three different reduction ratios for Delrin® and Tarnoform®, respectively. The recovery was based on the difference between the set roll gap and the thickness of the material exiting the rolls and the thickness of the start-up billet. The recovery curve for the three different R_As was identical suggesting unique recovery behaviour for a particular rolling temperature. After each rolling pass, the samples demonstrated significant recovery after exiting the deformation zone between the rolls. The recovery was more substantial at lower deformation but reduced at higher strains. This suggests the presence of a strong elastic component of strain in the material in the initial stages of the rolling process. However, higher deformation leads to a greater degree of plastic deformation that is not recoverable.

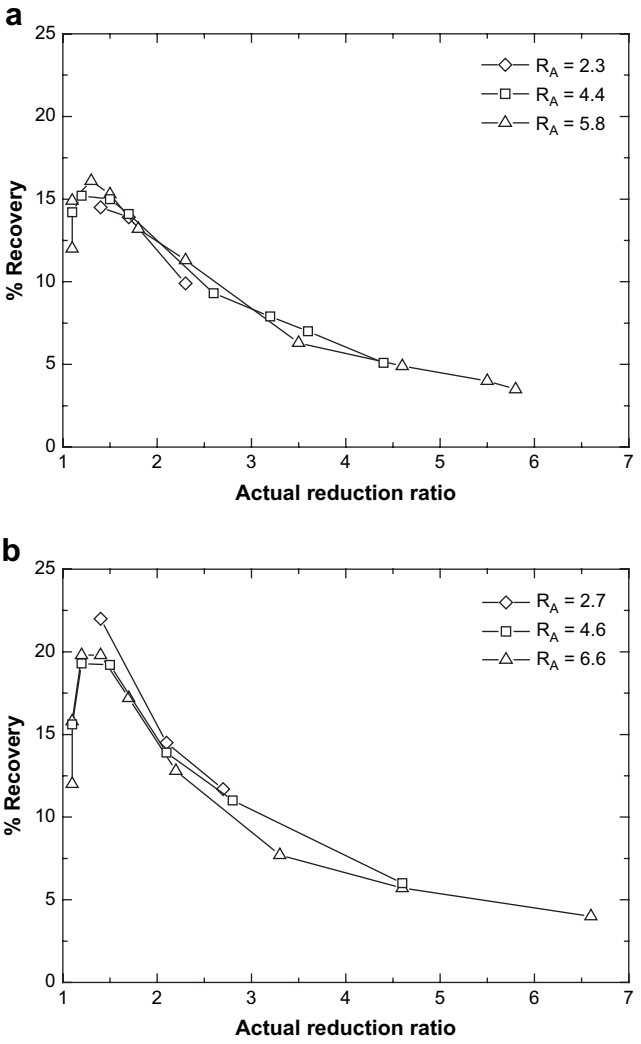

Fig. 5. The variation of the % recovery with the actual reduction ratio for (a) Delrin® rolled at 145 °C and (b) Tarnoform® rolled at a temperature of 135 °C.

3.4. Structure

3.4.1. WAXS

A number of studies have considered the crystal structure of polyoxymethylene with the aid of infrared spectroscopy, X-ray diffraction and electron diffraction [33–38]. Polyoxymethylene has been shown to exhibit polymorphism of crystal structure comprising both a hexagonal unit cell structure with a 9/5 (9 monomer units and 5 turns) helix [33] and an orthorhombic unit cell [33,39]. In this study, the WAXS patterns on isotropic and oriented Delrin® and Tarnoform® demonstrated that only the hexagonal unit cell structure with the 9/5 helix was present. The unit cell dimensions of the hexagonal structure for POM are $a = b = 4.45$ Å and $c = 17.3$ Å [33]. Because of this unit cell geometry, the a and b axes are in the same plane and perpendicular to the plane containing the c axis of the crystal, which corresponds to the direction of the molecular chain. The molecular chains are arranged in a 9/5 helix and aligned parallel to the c axis of the crystal [40].

The 2θ plot of non-deformed Delrin®, in the reflection mode, exhibited peaks at 22.9°, 34.5°, 48.2° and 54.1° correspond to the (100), (105), (115) and (205) lattice planes. The evolution of crystalline texture in the rolled samples was studied by X-ray pole figures for each crystallographic plane on samples machined perpendicular to the Force Direction (FD), Constraint Direction (CD) and Roll Direction (RD). Because of the hexagonal unit cell structure, information about the orientation of the molecular chains can be obtained from the (100) reflection because the normal to this plane is perpendicular to the c axis of the crystal, which is the direction of the molecular chains.

The idealised pole figures for the axial and the uniplanar-axial planes are illustrated in Fig. 6(a) and (b). In the case of the isotropic POM, the normal to the 4 lattice planes will be randomly oriented which would yield a figure with uniform intensity distribution. For axial orientation, the c axis of the unit cell will be parallel to the rolling direction and the a and b axes will be randomly distributed around the rolling direction. Because of the random distribution of the a and b axes around the c axis, the resultant pole figure of the four planes will be bands of uniform intensity. In the case of uniplanar-axial orientation, the c axis will be parallel to

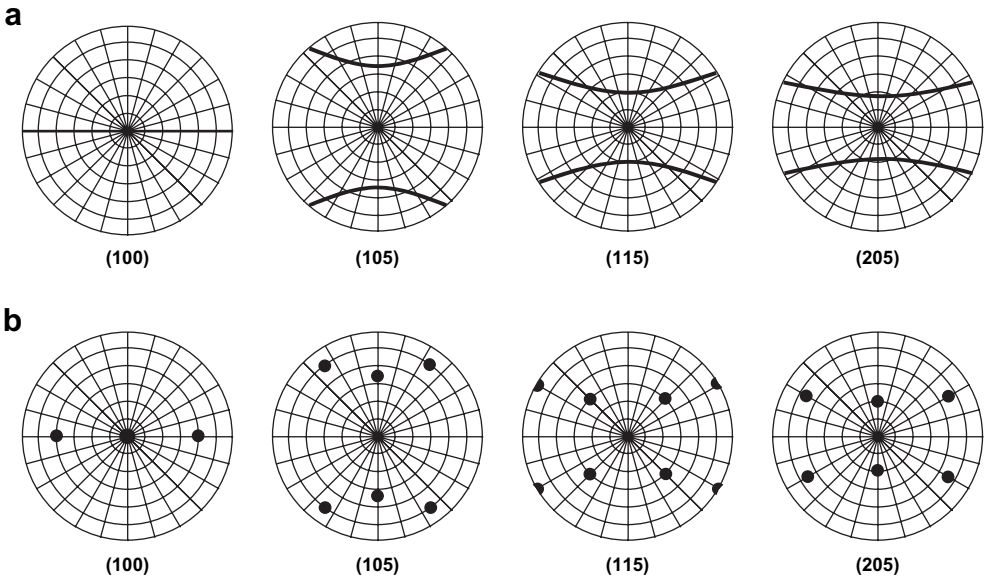

Fig. 6. Schematic representation of the ideal pole figures for polyoxymethylene subjected to (a) uniaxial and (b) uniplanar-axial orientations.

the rolling direction and the normal to the (100) plane will be parallel to FD. As shown in Fig. 6(b) such orientation will give rise to spots in the pole figures rather than bands. Pole figures, if properly constructed, contain quantitative data. In the pole figures in Figs. 7–9 the contour at the level 1.0 means the concentration of normals characteristic for random orientation. The contour at the level 2.0 means that the concentration is two times higher than that for the random distribution, contour at the level 3.0 means that the concentration is three times higher, etc. All areas below the contour 1.0 in pole figures mean the concentration of normals below random.

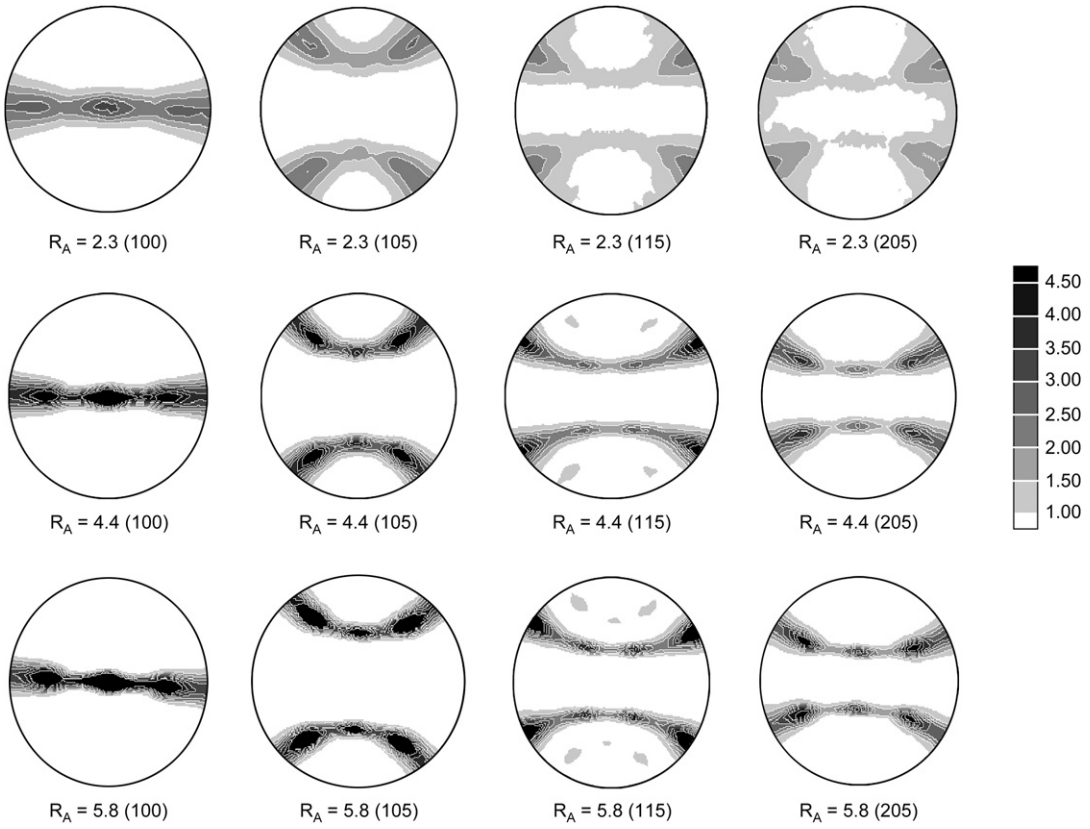

Fig. 7. Pole figures for oriented Delrin® at different reduction ratios and obtained with the incident X-ray beam parallel to the Force Direction (FD). The brackets in the figures refer to the lattice planes. A scale of concentration of normals to respective crystallographic planes, common for all pole figures in Figs. 7–9 is attached.

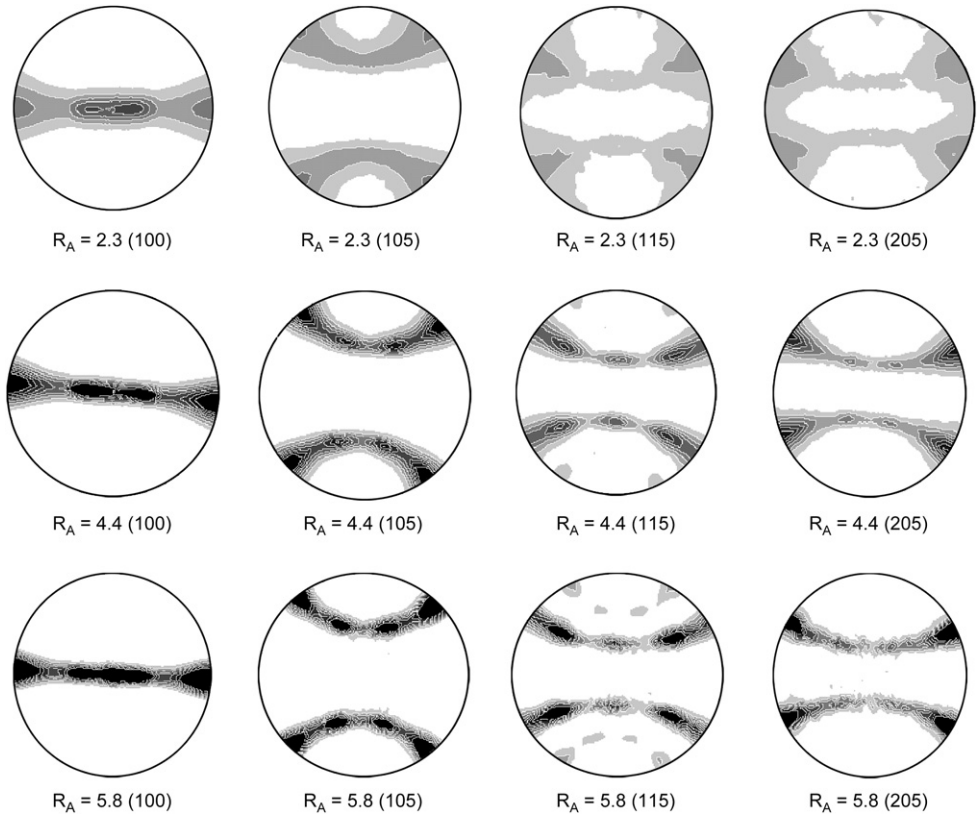

Fig. 8. Pole figures for oriented Delrin® at different reduction ratios obtained with the incident X-ray beam parallel to the Constraint Direction (CD). The brackets in the figures refer to the lattice planes. A scale of concentration of normals in Fig. 7 is attached.

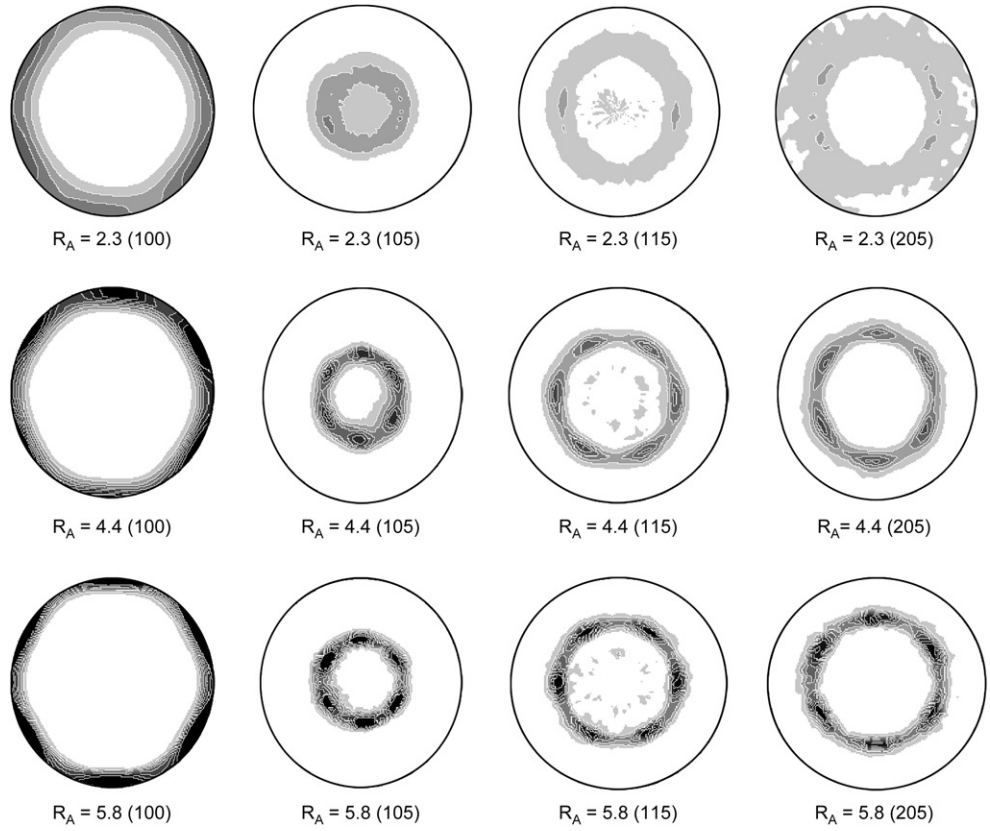

Fig. 9. Pole figures for oriented Delrin® at different reduction ratios obtained with the incident X-ray beam parallel to the Rolling Direction (RD). The brackets in the figures refer to the lattice planes. A scale of concentration of normals in Fig. 7 is attached.

The measured pole figures of (100), (105), (115) and (205) planes on a sample whose normal is parallel to the Force Direction (FD) for three different R_As are shown in Fig. 7. The pole figures for deformed Tarnoform® were similar to that of Delrin® for all the planes in all the directions and therefore only the latter case will be discussed here. It is clear from Fig. 7(a) that the texture sets in the material at a low R_A of 2.3. For very small deformation of POM by rolling, Starkweather et al. [40] noticed orientation of the molecular chains perpendicular to the rolling direction, which was attributed to the structural reorganisation during the initial stages of the deformation process. The present pole figures from the (100) plane showed a band along the equator with maxima at 60° from the centre, which corresponds to a combined axial and uniplanar-axial distribution of the crystallites. The bands and maxima for the (100) planes occurred along the equator of the pole figure that is indicative of the normals to the (100) planes distributed perpendicular to the orientation direction. The maxima were 60° apart because the angle between the normal of the adjacent unit cell faces of the hexagonal unit cell is 60° apart. Further constrained rolling led to the sharpening of the bands and an increased intensity of the spots along the equatorial direction indicating an increase in the degree of orientation of the crystalline phase. The concentration of normals in the maxima exceeded 4.5 times the concentration characteristic for random orientation of normals. The pole figures of the (105), (115) and (205) lattice planes also demonstrated bands and spots as do the (100) planes which confirm the presence of both uniaxial and uniplanar-axial orientations in this direction. The bands and maxima were offset from the equatorial plane because these planes are non-orthogonal to the chain direction, which also corresponds to the *c* axis of the crystal.

The orientation of the normals to the (100) plane perpendicular to the orientation direction suggests that such a texture is a result of the (100)[001] chain slip system, i.e., slip of the (100) plane along the chain direction [001]. The (100)[001] system is probably supported by the transverse slip systems such as the (010)[001]. However, more studies are required to determine the possible crystallographic deformation mechanisms. There have been reports of the transformation of the crystal phase from hexagonal to orthorhombic structure as a result of deformation [41], which has been attributed to the martensitic transformation due to stress [42]. There was no such evidence in the present study, which was confirmed by the WAXS and thermal analysis on the rolled samples.

The pole figures from the (100) plane for samples whose normal is parallel to the CD (Fig. 8) again showed bands and maxima along the equatorial direction (perpendicular to the orientation direction) but in this case the maxima appeared at the opposite edges of the sphere on either sides of the equator. This indicates that, in this direction, the *c* axis is parallel to the RD and the normal to the (100) planes is parallel to the FD. This was also confirmed by the presence of two maxima that are offset from the centre by 30° in the pole figures for $R_A = 2.3$ and 4.4. The pole figures from the (105), (115) and (205) lattice planes also showed bands and maxima that are indicative of the bimodal orientation systems.

The pole figures from the (100) lattice plane for samples whose normals are parallel to the RD (Fig. 9) showed 6 maxima along the circumference of the sphere that are 60° apart in the stereographic net. This is a result of the hexagonal unit cell structure of POM that has six type (*h*00) planes, the normals to which are 60° apart on a plane perpendicular to the *c* axis of the unit cell. The pole figures of the (105), (115) and (205) planes also demonstrated six-point patterns as shown in Fig. 9. It is evident from these pole figures that the *c* axes of the crystals are oriented along the RD and are perpendicular to the FD and CD. Similarly as for normals to (100) planes the concentration of normals to (105), (115) and (205) planes in the respective maxima exceeded 4.5 times the concentration characteristic for random orientation of normals.

3.4.2. SAXS

The SAXS patterns from the oriented Delrin® and Tarnoform® samples were similar and hence only the latter case will be presented here. The SAXS patterns for isotropic and rolled Tarnoform® at different reduction ratios are shown in Fig. 10. The SAXS patterns on the rolled samples were taken with the X-ray beam parallel to the Force Direction (FD) and Constraint Direction (CD). The SAXS pattern from the isotropic sample showed a broad isotropic ring suggesting that the crystalline lamellae are interspersed with amorphous layers in a periodic manner and have nearly isotropic orientation. A small intensity variation could also be noticed that suggests the existence of a weak orientation as a result of the melt extrusion process.

The SAXS pattern from the sample rolled to a R_A of 2.7 caused the ring with constant azimuthal intensity to reduce to a two-point pattern with the maxima oriented along the RD. These reductions of the isotropic ring to a two-point pattern suggest the transformation of the spherulitic morphology to a fibrillar structure. There was no evidence of microvoiding between the fibrils in this direction with increase in R_A. The intensity of the two-point pattern does not seem to decrease with increase in compression ratio, which suggests that there was no lamellar fragmentation for the orientation conditions and even the highest compression ratios considered in this study. In the case of HDPE [43], fragmentation of the lamellae was noticed for compression ratios greater than 3.1.

The SAXS patterns on a rolled sample when the X-ray beam was parallel to the CD for a R_A of 2.7 (Fig. 10) showed a broad ellipsoidal pattern with traces of isotropic material. There was no sign of lamellae fragmentation at low compression ratios. Increasing the compression ratio to 4.6 yielded a four-point pattern, which suggests cooperative kinking of the lamellae during deformation to produce a chevron-like structure. The intensity of the scattering pattern decreased with increase in R_A suggesting the destruction of the lamellae. In addition to the four-point pattern, there was faint diffused scattering along the equator, which originates from the microvoids. Between the rolls, the material is under a compressive stress field, which would inhibit void initiation. The evidence of microvoiding in the rolled material suggests that a small number of microvoids might have been initiated during the

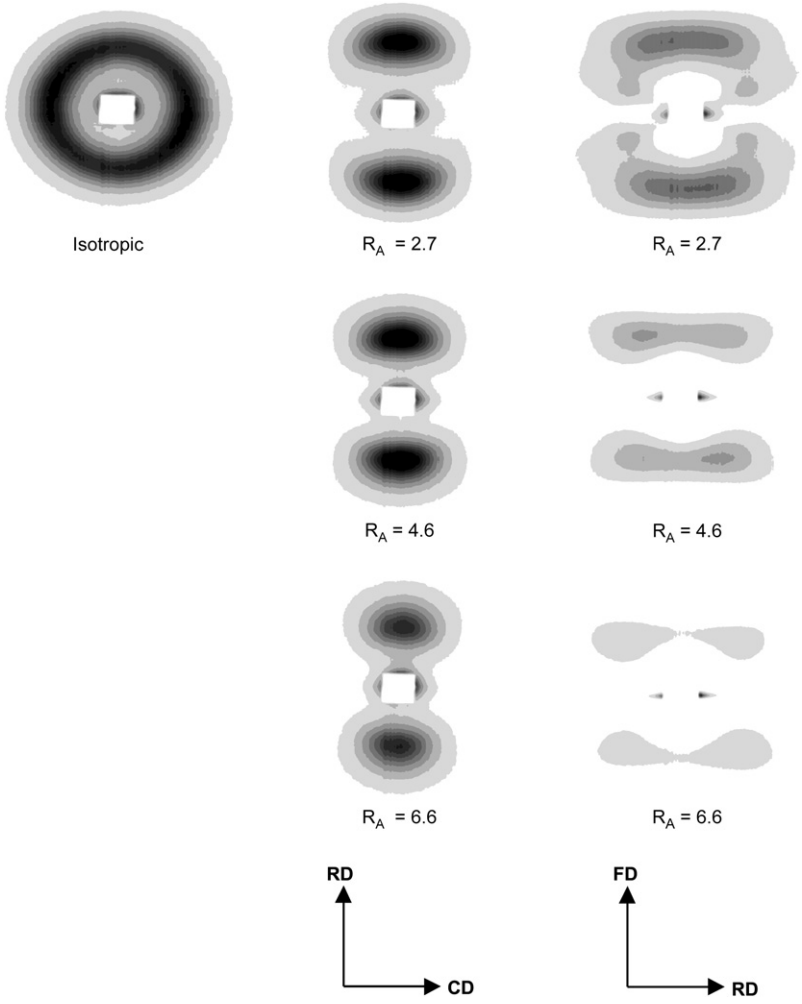

Fig. 10. SAXS patterns from isotropic and rolled Tarnoform®. SAXS patterns from rolled Tarnoform® were obtained at different actual reduction ratios.

strain recovery phase when the material exits the working zone between the rolls.

The orientation of the lamellar structure as inferred from the SAXS results of the rolled samples is schematically shown in Fig. 11. The two-point patterns obtained when the X-ray beam was parallel to the FD suggest the existence of fibre texture in this direction. The four-point patterns obtained when the X-ray beam was parallel to the CD suggest that the lamellar deformation in this direction is restricted to cooperative kinking. The existence of a bimodal structure has been addressed in detail by Bartczak and Lezak [44] for HDPE compressed in a channel die.

3.4.3. SEM

When thermoplastic polymers solidify, the crystallization in pockets of melt occluded by impinging spherulites is accompanied by a buildup of negative pressure due to the lower specific volume of the solidified material [45–52]. The negative pressure can grow to a certain limit, beyond which cavitation occurs and the melt fractures. Microvoids formed in crystallizable polymers during their solidification undoubtedly lower their mechanical performance. In Ref. [50] it was shown that the microvoiding during crystallization of POM is similar to cavitation phenomena typical for other polymers. Large cavities are frequently found in extruded or injection moulded

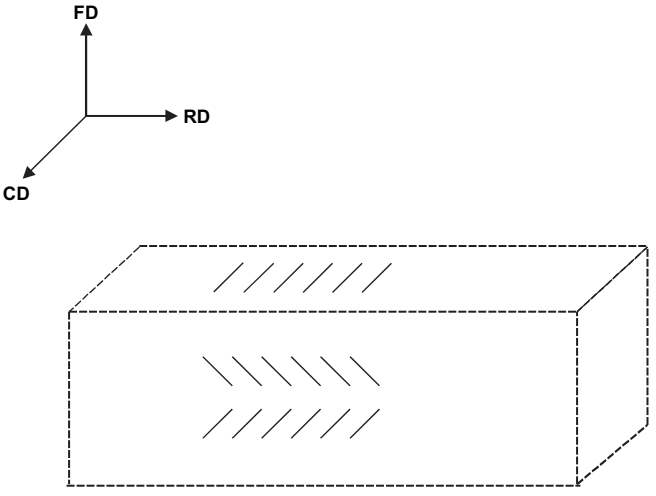

Fig. 11. Schematic of the lamellae organisation during constrained rolling of polyoxymethylene as inferred from the SAXS results.

POM components [e.g. [52]] which indicate the importance of the cavitation phenomena in this polymer, whose high crystallinity level and high volume change during crystallization facilitate negative pressure buildup and cavitation. During crystallization in occluded pockets of melt, numerous microvoids usually appear synchronously at the spherulite–melt interface. It has previously been suggested [51,53] that the synchronous appearance of the microvoids could be a combined effect of the superposition of the negative pressure inside a weak spot and the acoustic wave produced by the primary cavitation event. Acoustic emission due to cavitation during polymer crystallization has in fact been evidenced in the past by Galeski et al. [46]. Recently, the cavitation during crystallization of POM was studied in Ref. [54]. The POM billets used in the present work were obtained by extrusion of 16 mm thick sheets. Crystallization of such thick sheets occurs slowly and starts from the outer layers. The volume deficiency accumulates and certainly the condition for cavitation in occluded pockets of melt is satisfied.

A SEM micrograph of a liquid nitrogen fractured Delrin® sample is seen in Fig. 12 where quite large and numerous cavities are visible. When the sample is rolled the cavities are squeezed into flat discs. The compressed cavities are clearly seen as long narrow openings in the CD view of the rolled sample presented in the SEM micrograph of Fig. 13. These features were further visualized by etching as presented in Fig. 14(a and b). Compressed cavities are now visible as open fissures in Fig. 14(a) where the FD view of an etched rolled Delrin® sample is shown. The CD view of the same etched Delrin® sample in Fig. 14(b) demonstrates the evidence of microcracks parallel to the flow direction as a result of uniplanar-axial orientation of the material during rolling. Rolling also caused a transformation from a spherulitic morphology to a highly deformed laminar structure resembling a stack of paper, with the stacks aligned parallel to the Rolling Direction (RD). Sporadic cavities, which were present in the pristine material, were also compressed and they can be found occasionally between the strands. They could lead to easier delamination of the rolled material along the FD–CD planes.

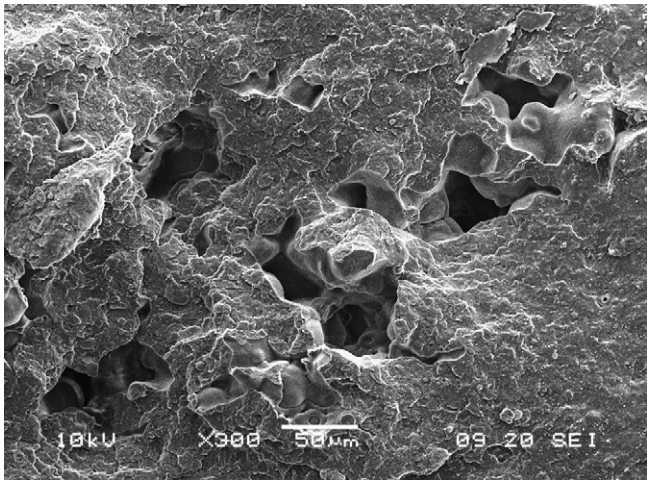

Fig. 12. SEM micrograph of liquid nitrogen fractured isotropic Delrin®.

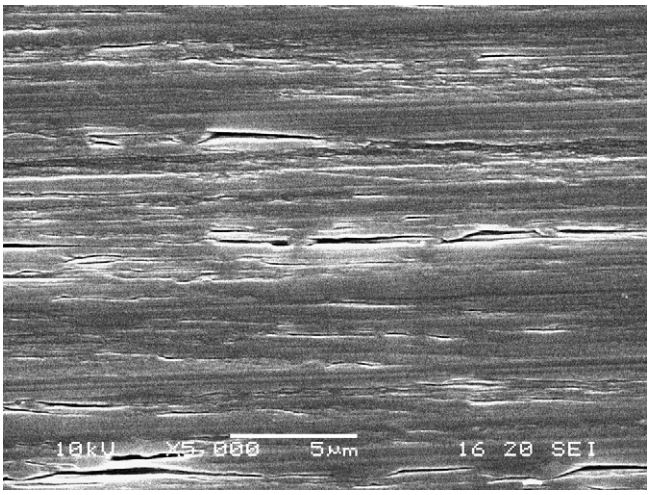

Fig. 13. SEM micrographs of the surface of Delrin® rolled to $R_A = 5.8$. View from the Constraint Direction (CD).

3.5. Tensile modulus

Fig. 15 shows the modulus of the rolled samples measured in tension parallel to the orientation (rolling) direction. The

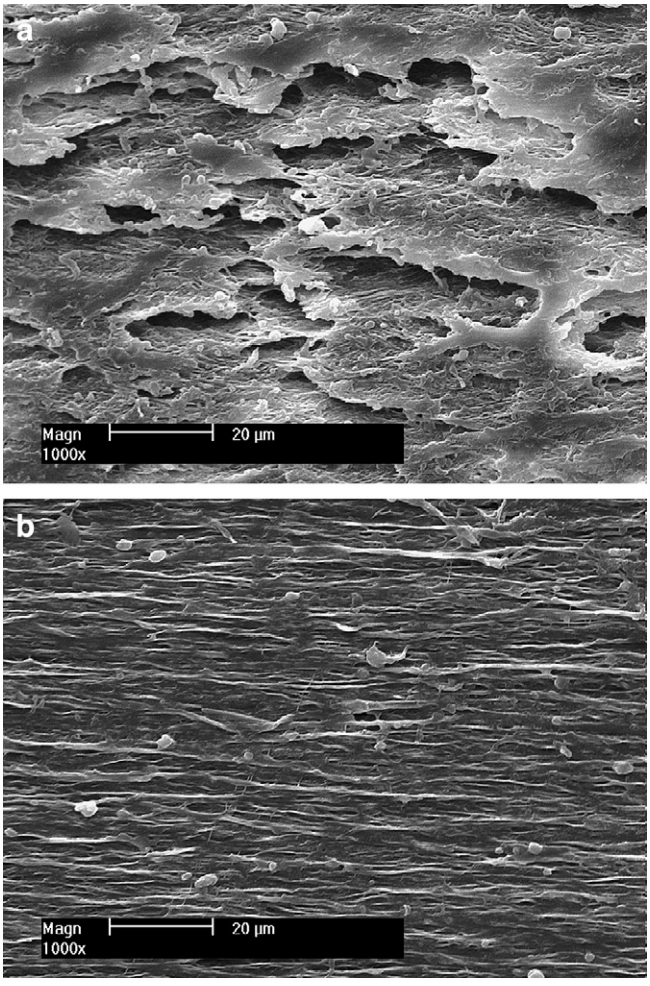

Fig. 14. SEM micrographs of the etched surface of Delrin® rolled to $R_A = 5.8$. (a) View from the Force Direction (FD) and (b) view from Constraint Direction (CD).

figure shows that the modulus of both the resins increased almost linearly with reduction ratio. The enhancement in modulus with R_A is as a result of increase in orientation of both the crystalline and amorphous phases with R_A. For all the reduction ratios considered in this study, Delrin® demonstrated higher modulus than Tarnoform®, the difference being around 20% at a R_A of 4.4.

3.6. Tensile strength

Fig. 16 shows the tensile strength of the rolled Delrin® and Tarnoform® measured parallel to the orientation direction. The strength of both the resins increased proportionally with R_A as a result of increase in amorphous and crystalline orientations. Rolled Delrin® exhibited higher strength than rolled Tarnoform®. The strength, unlike the modulus, is influenced by morphological factors such as the presence of voids. In the case of POM, it was recently shown [52] that the strength of oriented samples from the hydrostatic extrusion process is greater than that of the corresponding oriented samples produced by die-drawing for draw ratios greater than 4. The reduction in strength can be attributed to the existence of voids in the die-drawn material, as a result of the tensile nature of the process. Similar observations have also been made for POM that was freely drawn under both ambient and hydrostatic pressures [9]. In the present case, the strength increased almost linearly with R_A, which suggests that the morphological damage was minimised due to the compressive nature of the constrained rolling process.

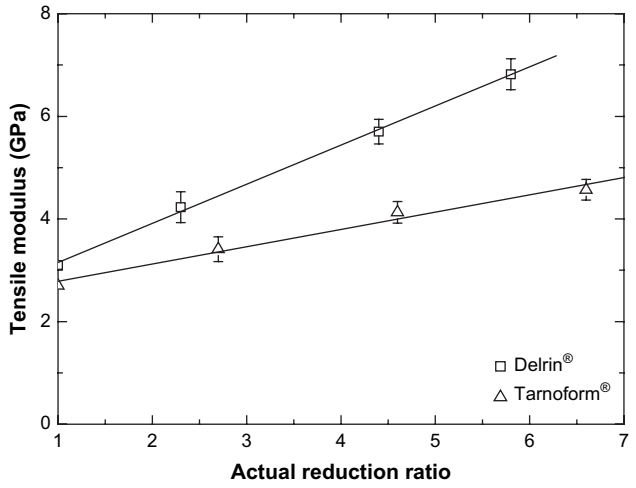

Fig. 15. The variation of the tensile modulus with the actual reduction ratio for Delrin® and Tarnoform® oriented using the constrained rolling process.

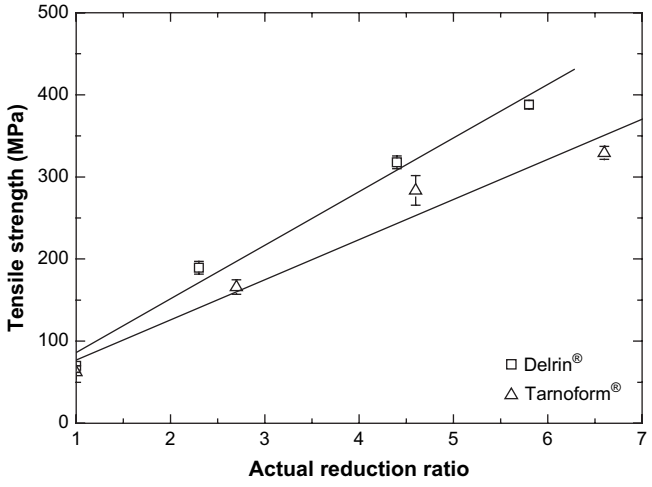

Fig. 16. The variation of the tensile strength with the actual reduction ratio for Delrin® and Tarnoform® oriented using the constrained rolling process.

3.7. Impact tests

Photographs of the fractured samples with the initial notch parallel to the Force Direction (FD) are shown in Fig. 17. The sample oriented to R_A of 2.3 failed completely but the crack propagated along the length of the sample, i.e., perpendicular to the axis of loading. At R_A of 4.4, the fracture process was incomplete with the specimens exhibiting a hinge type break and with the specimens still held intact; this is described as ''H-type failure'' according to the ISO standard 179 [55]. The primary crack bifurcated causing subsidiary cracks to propagate parallel to the RD but their growth was arrested due to the planar orientation as a result of rolling. As there was no propagation of the primary crack, the results have

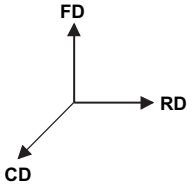

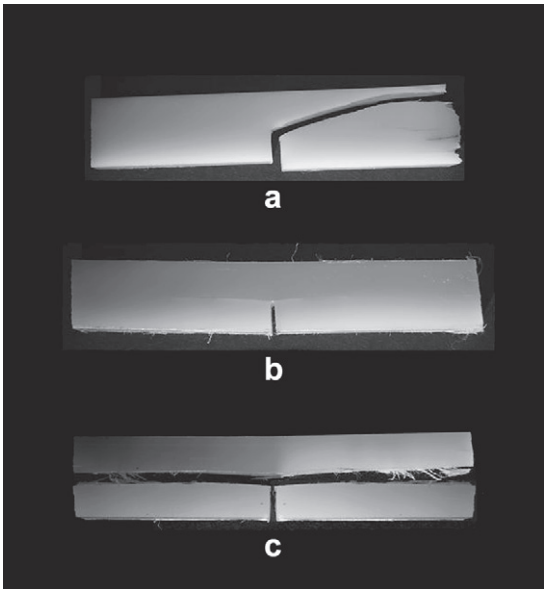

Fig. 17. The photograph showing the rolled Delrin® samples after the impact tests. The samples were rolled to reduction ratios of (a) 2.3, (b) 4.4 and (c) 5.8. The initial notch was parallel to the Force Direction (FD).

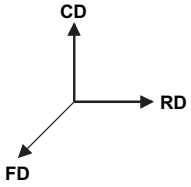

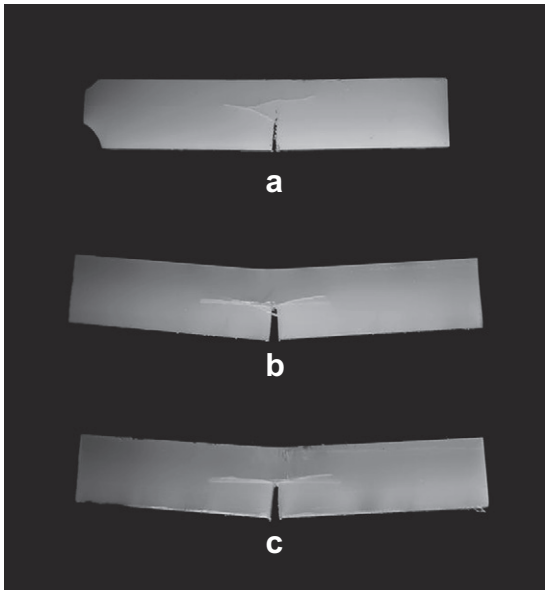

Fig. 18. The photograph showing the rolled Delrin® samples after the impact tests. The samples were rolled to reduction ratios of (a) 2.3, (b) 4.4 and (c) 5.8. The initial notch was parallel to the Constraint Direction (CD).

only been assessed qualitatively. The damage zone in this case is reminiscent of that of a unidirectional fibre composite [56,57], when the initial crack was perpendicular to the principle fibre or orientation direction.

The crack tip blunting mechanism in anisotropic materials with the crack growing perpendicular to the orientation direction was addressed by Cook et al. [58] according to whom two components of stress act at the vicinity of the crack tip. In addition to the stress acting along the loading direction, secondary stresses are generated perpendicular to the loading direction. In an anisotropic material, because of the reduction in the transverse strength, secondary cracks tend to open and these blunt and deflect the main crack to follow the weaker direction. This deflection of the main crack by the generation of secondary cracks has been viewed as a mechanism for increasing material toughness [56–59].

Increasing R_A to 5.8 caused the sample to split perpendicular to the axis of loading, i.e., along the rolling direction, due to the increase in the level of molecular orientation along the RD. The toughness in this direction can be inferred from the size of the damage zone ahead of the primary crack. From the photographs of the fractured samples in Fig. 17, it can be concluded that the sample oriented to R_A of 4.4 exhibited higher toughness than those oriented to $R_A = 2.3$ or 5.8.

The photographs of the fractured samples with the initial notch parallel to the CD are shown in Fig. 18. As observed in the previous case, the fracture process was incomplete with the primary crack bifurcating to produce secondary cracks perpendicular to the loading direction, i.e., parallel to the RD. From the size of the damage zone near the crack tip, it can be inferred that the toughness increases with increase in R_A.

4. Conclusions

Optimum conditions for the constrained rolling of polyoxymethylene were established based on channel die plane strain compression tests. Both homopolymer (Delrin®) and copolymer (Tarnoform®) were successfully processed to reduction ratios in excess of 5. Texture analysis by means of WAXS revealed the existence of both uniaxial and planar orientations of the crystallites at low reduction ratios while for high ratios only uniplanar texture was detected. The orientation of the normals to the (100) plane perpendicular to the orientation direction suggests that such a texture is a result predominantly of the (100)[001] chain slip system. SAXS analysis led to the conclusion that the lamellae did not fragment during compression but an extensive lamellae kinking was present resulting in a chevron-like lamellar structure in the rolled samples when viewed along the constraint direction.

Modulus and strength parallel to the rolling direction increased almost linearly with compression ratio. The homopolymer Delrin® deformed to a reduction ratio of 5.8 attained a tensile strength of nearly 400 MPa and a modulus of nearly 7 GPa while the copolymer Tarnoform® deformed to a reduction ratio of 6.5 is characterized by a tensile strength of over 300 MPa and a modulus of over 4 GPa. Impact tests on the rolled samples with the notch parallel to the force and constraint direction resulted in incomplete fracture but the results indicate that the fracture energy increases with reduction ratio. The enhancement in properties as a result of molecular orientation under constrained rolling conditions suggests that these materials can have major commercial applications.

Acknowledgements

The British Council and the Polish Ministry of Scientific Research and Information Technology are acknowledged for partial support of J. Mohanraj while visiting the Centre of Molecular and Macromolecular Studies, Polish Academy of Sciences. The Engineering and Physical Sciences Research Council (Grant no: GR/R80087/01) is also acknowledged.

References

[1] Ward IM. Advances in Polymer Science 1985;70:1–70.
[2] Zachariades AE, Porter RS. High modulus polymers: approaches to design and development. New York: Marcel Dekker; 1988.
[3] Ward IM. Structure and properties of oriented polymers. London: Chapman & Hall; 1997.
[4] Ward IM, Coates PD, Dumoulin MM. Solid phase processing of polymers. Munich: Hanser Gardner; 2000.
[5] Galeski A. Progress in Polymer Science 2003;28(12):1643–99.

[6] Schaffner F, Vinson J, Jungnickel BJ. Angewandte Makromolekulare Chemie 1991;185:137–45.
[7] Ward IM, Sweeney J. An introduction to the mechanical properties of solid polymers. 2nd ed. Chichester: Wiley; 2004.
[8] Taraiya AK, Mirza MS, Mohanraj J, Barton DC, Ward IM. Journal of Applied Polymer Science 2003;88(5):1268–78.
[9] Komatsu T, Enoki S, Aoshima A. Polymer 1991;32(11):1988–93.
[10] Mohanraj J, Barton DC, Ward IM, Dahoun A, Hiver JM, G'Sell C. Polymer 2006;47(16):5852–61.
[11] Hope PS, Richardson A, Ward IM. Journal of Applied Polymer Science 1981;26(9):2879–96.
[12] Capaccio G, Ward IM. British Patent Appl. 52644/74 and cogs. filed. United Kingdom: United Kingdom Patents Specification; 1973.
[13] Clark ES, Scott LS. Polymer Engineering and Science 1974;14(10): 682–6.
[14] Brew B, Ward IM. Polymer 1978;19(11):1338–44.
[15] Komatsu T, Aoshima A. Journal of Polymer Science, Part B: Polymer Physics 1995;33(2):179–87.
[16] Zihlif AM. Materials Chemistry and Physics 1985;13(1):21–45.
[17] Komatsu T, Enoki S, Aoshima A. Polymer 1991;32(16):2992–4.
[18] Komatsu T, Enoki S, Aoshima A. Polymer 1991;32(11):1994–9.
[19] Takeuchi Y, Yamamoto F, Konaka T, Nakagawa K. Journal of Polymer Science, Part B: Polymer Physics 1986;24(5):1067–77.
[20] Komatsu T, Enoki S, Aoshima A. Polymer 1991;32(11):1983–7.
[21] Mohanraj J, Barton DC, Ward IM, submitted for publication.
[22] Hosford WF, Caddell RM. Metal forming: mechanics and metallurgy. 2nd ed. London: Prentice-Hall; 1993.
[23] Morawiec J, Bartczak Z, Kazmierczak T, Galeski A. Materials Science and Engineering A – Structural Materials Properties Microstructure and Processing 2001;317(1–2):21–7.
[24] Bartczak Z. Journal of Applied Polymer Science 2002;86(6):1396–404.
[25] Bartczak Z, Morawiec J, Galeski A. Journal of Applied Polymer Science 2002;86(6):1405–12.
[26] Bartczak Z, Morawiec J, Galeski A. Journal of Applied Polymer Science 2002;86(6):1413–25.
[27] Pluta M, Bartczak Z, Galeski A. Polymer 2000;41(6):2271–88.
[28] Ajji A, Dumoulin MM, Cole KC. Engineering Plastics 1996;9(3):216–24.
[29] Chapleau N, Mohanraj J, Ajji A, Ward IM. Polymer 2005;46(6): 1956–66.
[30] Williams JG, Cawood MJ. Polymer Testing 1990;9(1):15–26.
[31] Iguchi M. Die Makromolekulare Chemie 1976;177(2):549–66.
[32] Crane FAA, Alexander JM. Journal of the Institute of Metals 1963;91(5):188–9.
[33] Carazzolo GA. Journal of Polymer Science, Part A: General Papers 1963;1(5):1573.
[34] Rickert SE, Baer E. Journal of Applied Physics 1976;47(10):4304–9.
[35] Saruyama Y, Miyaji H, Asai K. Journal of Polymer Science, Part B: Polymer Physics 1979;17(7):1163–70.
[36] Balik CM, Tripathy SK, Hopfinger AJ. Journal of Polymer Science, Part B: Polymer Physics 1982;20(11):2003–16.
[37] Hama H, Tashiro K. Polymer 2003;44(22):6973–88.
[38] Tashiro K, Kamae T, Asanaga H, Oikawa T. Macromolecules 2004; 37(3):826–30.
[39] Carazzolo G, Leghissa S, Mammi M. Makromolekulare Chemie 1963; 60:171–90.
[40] Starkweather Jr HW, Wilson FC, Clark ES. Journal of Polymer Science, Part B: Polymer Letters 1971;9(8):623–5.
[41] Preedy JE, Wheeler EJ. Nature – Physical Science 1972;236(65):60.
[42] Harris N, Bevis M. Journal of Materials Science 1975;10(3):539–41.
[43] Galeski A, Bartczak Z, Argon AS, Cohen RE. Macromolecules 1992;25(21):5705–18.
[44] Bartczak Z, Lezak E. Polymer 2005;46(16):6050–63.
[45] Galeski A, Piorkowska E. Journal of Polymer Science, Part B: Polymer Physics 1983;21(8):1313–22.
[46] Galeski A, Koenczoel L, Piorkowska E, Baer E. Nature 1987;325(6099): 40–1.
[47] Galeski A, Piorkowska E, Koenczoel L, Baer E. Journal of Polymer Science, Part B: Polymer Physics 1990;28(7):1171–86.
[48] Pawlak A, Galeski A. Journal of Polymer Science, Part B: Polymer Physics 1990;28(10):1813–21.
[49] Thomann R, Wang C, Kressler J, Mulhaupt R. Macromolecular Chemistry and Physics 1996;197(3):1085–91.
[50] Pawlak A, Piorkowska E. Journal of Applied Polymer Science 1999;74(6):1380–5.
[51] Nowacki R, Kolasinska J, Piorkowska E. Journal of Applied Polymer Science 2001;79(13):2439–48.
[52] Mohanraj J, Bonner MJ, Barton DC, Ward IM. Polymer 2006;47(16): 5897–908.
[53] Varga J, Ehrenstein GW. Polymer 1996;37(26):5959–63.
[54] Nowacki R, Piorkowska E. Journal of Applied Polymer Science 2007;105(3):1053–62.
[55] Plastics: determination of Charpy impact properties. Non-instrumented impact test; 2001.
[56] Beaumont PWR, Anstice PD. Journal of Materials Science 1980;15(10): 2619–35.
[57] Sova M, Raab M, Slizova M. Journal of Materials Science 1993;28(23): 6516–23.
[58] Cook J, Evans CC, Gordon JE, Marsh DM. Proceedings of the Royal Society of London, Series A – Mathematical and Physical Sciences 1964;282(139):508–20.
[59] Deanin RD, Crugnola AM. Toughness and brittleness of plastics. Washington: American Chemical Society; 1976.